Suppression of the Nonlinear Zeeman Effect and Heading Error in Earth-Field-Range Alkali-Vapor Magnetometers

Guzhi Bao,[1,2] Arne Wickenbrock,[1] Simon Rochester,[3] Weiping Zhang,[4,5] and Dmitry Budker[1,6,7,8]
[1]Johannes Gutenberg-Universität Mainz, 55128 Mainz, Germany
[2]Department of Physics, East China Normal University, Shanghai 200062, China
[3]Rochester Scientific, LLC, El Cerrito, California 94530, USA
[4]School of Physics and Astronomy, Shanghai Jiao Tong University, and Tsung-Dao Lee Institute, Shanghai 200240, China
[5]Colleaborative Innovation Center of Extreme Optics, Shanxi University, Taiyuan, Shanxi 030006, China
[6]Helmholtz Institut Mainz, 55099 Mainz, Germany
[7]Department of Physics, University of California, Berkeley, California 94720-7300, USA
[8]Nuclear Science Division, Lawrence Berkeley National Laboratory, Berkeley, California 94720, USA

(Received 1 September 2017; published 17 January 2018)

The nonlinear Zeeman effect can induce splitting and asymmetries of magnetic-resonance lines in the geophysical magnetic-field range. This is a major source of "heading error" for scalar atomic magnetometers. We demonstrate a method to suppress the nonlinear Zeeman effect and heading error based on spin locking. In an all-optical synchronously pumped magnetometer with separate pump and probe beams, we apply a radio-frequency field which is in phase with the precessing magnetization. This results in the collapse of the multicomponent asymmetric magnetic-resonance line with ~100 Hz width in the Earth-field range into a single peak with a width of 22 Hz, whose position is largely independent of the orientation of the sensor within a range of orientation angles. The technique is expected to be broadly applicable in practical magnetometry, potentially boosting the sensitivity and accuracy of Earth-surveying magnetometers by increasing the magnetic-resonance amplitude, decreasing its width, and removing the important and limiting heading-error systematic.

DOI: 10.1103/PhysRevLett.120.033202

High-sensitivity magnetometers are used in a wide variety of applications ranging from geophysics [1] to fundamental physics [2,3] and to medicine [4,5]. Alkali-metal-vapor atomic magnetometers have seen tremendous progress in recent years, improving their sensitivities to below the $\mathrm{fT}/\sqrt{\mathrm{Hz}}$ level for submicrotesla fields [1,6–9]. However, in the geophysical field range (up to 100 μT), the nonlinear Zeeman (NLZ) effect [10–13] can cause splitting of the different magnetic-resonance components and produce line shape asymmetries. This leads to a signal reduction and a spurious dependence of the scalar-sensor readings on the relative orientation of the sensor and magnetic field. This important systematic effect is called a heading error [14,15] and becomes particularly troublesome in airborne and marine systems.

Recently, NLZ shifts have been canceled using several different approaches: double-modulated synchronous optical pumping [10], high-order polarization moments [11], and tensor light-shift effects [12]. Here, we introduce an alternative technique that is more generally applicable and easier to implement. It involves "locking" the atomic spins with an additional radio-frequency (rf) field to suppress the NLZ effect and as a result also the heading error. Spin locking is often used in nuclear magnetic-resonance (NMR) experiments to prevent the precession or decay of the nuclear magnetization [16]. In atomic systems, spin locking prevents splitting, shifts, and line shape asymmetries. In contrast to other schemes, spin-locked magnetometers are more robust against orientation changes.

For states with electronic angular momentum $J = 1/2$, the energies of the magnetic sublevels $|m\rangle$ of a state with total angular momentum F as a function of the magnetic field are given by the Breit-Rabi formula [17,18]:

$$E_m = -\frac{\Delta_{\mathrm{hf}}}{2(2I+1)} - g_I \mu_B m B \pm \frac{\Delta_{\mathrm{hf}}}{2}\left(1 + \frac{4m\xi}{2I+1} + \xi^2\right)^{1/2}, \quad (1)$$

where $\xi = (g_J + g_I)\mu_B B/\Delta_{\mathrm{hf}}$, g_J and g_I are the electronic and nuclear Landé factors, respectively, B is the magnetic-field strength, μ_B is the Bohr magneton, Δ_{hf} is the hyperfine-structure interval, I is the nuclear spin, and the $\pm$ refers to the $F = I \pm 1/2$ hyperfine components. The eigenenergies are shown in Fig. 1(a) as a function of the magnetic-field strength. It follows from Eq. (1) that the $\Delta m = \pm 1$ Zeeman-transition frequencies in both manifolds are m

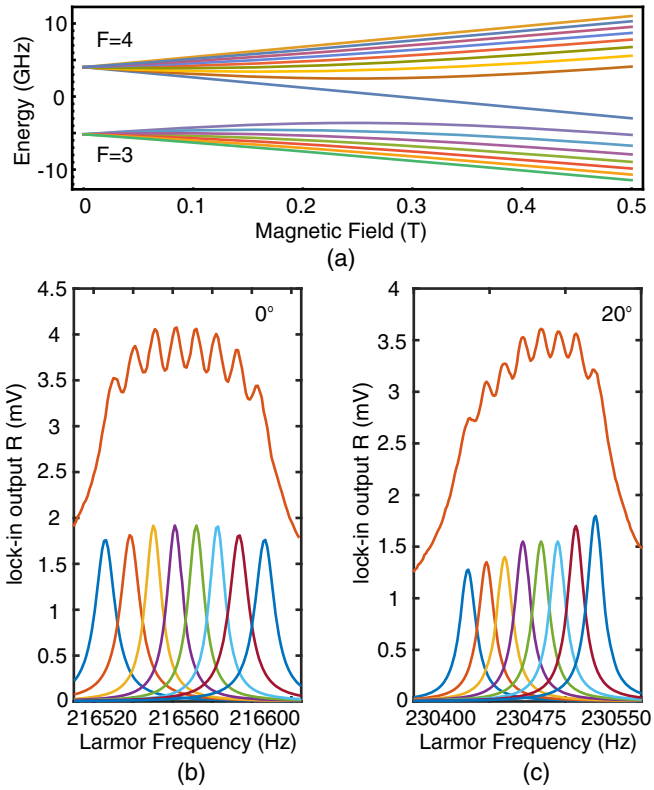

FIG. 1. (a) Hyperfine structure of the Cs ground state manifolds in an external magnetic field. In this work, we are concerned with fields that correspond to $\sim 10^{-4}$ of the shown range, where the NLZ effect is a small perturbation. (b) Optical-rotation signal amplitude (see Fig. 2) from the lock-in amplifier for a fixed pump-modulation frequency of 216 560 Hz and a sweep of the magnetic field (given in Larmor frequency of the magnetic resonance neglecting NLZ shifts). The central field is $B \approx 62\ \mu$T. The data are fit with eight Lorentzian peaks arising due to the NLZ effect. (c) The same data collected with a 20° tilt of the sensor and a pump-modulation frequency of 230 475 Hz.

dependent with the difference dependent on B. In the Earth-field range, these contributions are already substantial. Therefore, for the experiments presented here, we expand the eigenenergies to second order in the magnetic field B. For the $\mathrm{Cs}6^2S_{1/2}F = 4$ state, the transition frequencies between adjacent Zeeman sublevels are then given by

$$\omega_{F,m} \approx \frac{\mu_B B}{4\hbar} + \omega_{\mathrm{rev}}(2m-1), \tag{2}$$

where $\omega_{\mathrm{rev}} = (\mu_B B)^2/(16\hbar\Delta_{\mathrm{hf}})$ is the quantum-beat revival frequency (see, for example, Ref. [18]). In Earth's magnetic field (typically 50 μT), this frequency for Cs is $\omega_{\mathrm{rev}} = 2\pi \times 3.3$ Hz and comparable to the low-field magnetic-resonance width for the vapor cell used in this experiment. Therefore, our magnetometer is strongly affected by the nonlinear Zeeman effect at magnetic fields at the level of Earth's field. As shown in the data presented in Figs. 1(b) and 1(c), the magnetic resonance is split into eight peaks. The linewidth for each peak is 9 Hz, but the effective linewidth of the NLZ-split magnetic resonance is 120 Hz. The broadening of the resonance reduces magnetic sensitivity. Another effect, also visible in the data presented in Fig. 1(c), occurs when the sensor is not properly oriented with respect to the magnetic field. Instead of a symmetric distribution of the peaks, a pronounced asymmetry appears when the magnetic field is not perpendicular to the pump and probe beams. This effect is called a *heading error* and leads to a systematic false reading of the magnetic field, which limits the usability of optical magnetometers, for example, in airborne-exploration applications in Earth's field.

If spins are initially oriented at an angle to the magnetic field, they precess around the magnetic field with frequency ω_L. However, in the presence of NLZ, the evolution of the spins is more complex than just spin precession and is characterized by the interconversion of different precessing polarization moments leading to periodic disappearances and revivals of orientation. The effect can be modeled as a periodic conversion among polarization moments, such as orientation-to-alignment conversion (OAC) [18] as discussed in Supplemental Material [19]. The main idea of our method is to provide a small locking magnetic field in the rotating frame along the direction of the main spin component. This prevents the spins from undergoing OAC, by forcing them to precess around this auxiliary field. If the Larmor frequency associated to this spin-locking field is much larger than the revival frequency ω_{rev}, the nonlinear Zeeman effect is compensated.

The experimental setup is shown in Fig. 2. A paraffin-coated cylindrical cell [22–25] at room temperature with 4 cm diameter and 5 cm length containing ^{133}Cs is enclosed within a four-layer mu-metal magnetic shield. A $-\hat{y}$-directed, circularly polarized pump beam is locked to the $\mathrm{Cs}D2 6^2S_{1/2}F = 3 \rightarrow 6^2P_{3/2}F' = 4$ transition at 852 nm with a dichroic atomic vapor laser lock [26]. A static magnetic field up to 100 μT is applied along $\hat{z}$; an oscillating magnetic field can be applied along $\hat{y}$ using coils within the inner shield. Additional dc magnetic fields can also be applied along $\hat{x}$ and $\hat{y}$ to tilt the total field away from $\hat{z}$ to study the heading error. The polarization of a 10 μW, $-\hat{x}$-directed, linearly polarized probe beam detuned by 4 GHz to the blue from the $\mathrm{Cs}D2F = 4 \rightarrow F' = 5$ transition is measured with a balanced polarimeter upon transmission through the cell.

The pump beam is intensity modulated (3% duty cycle) with an acousto-optic modulator (AOM). The light power during the "on" part of the cycle is 50 μW. We fix the modulation frequency at a particular value and scan the leading magnetic field until the polarization oscillation frequency is resonant with the Larmor precession, as detected via the maximum polarization rotation amplitude of the probe beam [27]. The signal from the balanced polarimeter is fed into a lock-in amplifier and demodulated

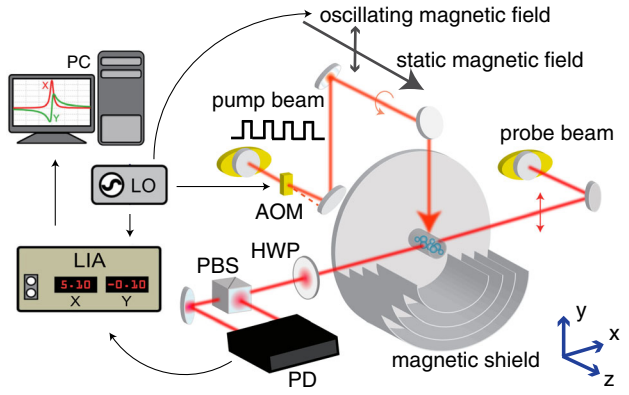

FIG. 2. Experimental setup. AOM, acousto-optic modulator used to pulse the pump beam; HWP, half-wave plate; PBS, polarizing beam splitter; PD, balanced photodetector; LIA, lock-in amplifier; LO, local oscillator. Atoms are contained in a vapor cell positioned in the center of the magnetic shield and are pumped and probed by laser beams under a static (along $\hat{z}$) and an oscillating magnetic field (along $\hat{y}$). A partial view of the magnetic shield is shown in the figure.

at the modulation frequency. Examples of experimental scans are shown in Fig. 3. In the absence of the spin-locking rf field, the magnetic resonance is composed of eight Lorentzian peaks with a width of 14.7 Hz each. Applying the rf field compresses all the different Lorentzians into a 21.8-Hz-wide central peak with a 3.4× increased amplitude.

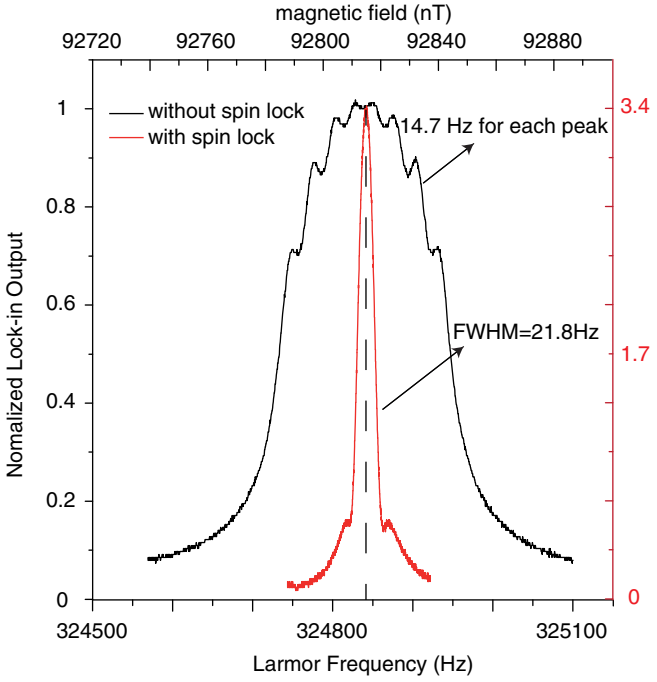

FIG. 3. Normalized magnetic-resonance data for a pump-modulation frequency of 324 840 Hz as a function of the leading magnetic field along the $\hat{z}$ axis with (red, right vertical scale) and without (black, left vertical scale) an applied spin-locking rf field.

To provide the spin-locking field, a sinusoidal current derived from the same function generator that modulates the pump-beam intensity is applied to the magnetic field coils in the $\hat{y}$ direction. By using the internal control of the local oscillator and adjusting the phase ϕ between the pumping pulses and the oscillating magnetic field, the effective direction of the static magnetic field in the rotating frame (spanned by $\hat{x}'$, $\hat{y}'$) can be changed like $\cos(\phi)\hat{x}' + \sin(\phi)\hat{y}'$, where $\hat{y}'$ points along the magnetization.

Figure 3 shows the amplitude of the lock-in output as a function of the leading magnetic field around 92 μT with the pump-laser modulation frequency fixed at 324 840 Hz. The data are presented without and with applying the spin-locking field in black and red, respectively. For this field, the spin-locking field is applied along $\hat{y}$ and has a 5.4 nT root-mean-square (rms) amplitude. The phase of the spin-locking field with respect to the pump-modulation signal is optimized by maximizing the lock-in signal (R) in the center of the resonance. With a spin-locking field, the amplitude of the optical rotation signal is 3.4 times larger, while the effective linewidth of the central peak is an order of magnitude smaller. If the atomic spins are locked, ideally only one Larmor frequency exists in the system. The magnetic resonance should have the same amplitude and linewidth at low and high fields. Experimentally, however, the linewidth is broader at high fields [21.85(7) Hz] than at low fields [3.94(4) Hz]. We attribute this difference to power broadening by the oscillating field when high fields are applied. Plots illustrating the linewidth dependence on the rf power and the signal line shape for different values of the phase are presented in Supplemental Material [19].

Figure 4(a) shows the lock-in output for a tilt angle of 10° without and with a spin-locking field. About 10 μT misalignment field is applied along the $\hat{x}$ direction, tilting the overall magnetic field towards the probe beam. As shown in Fig. 1, this shifts the weight of the individual magnetic resonances. This causes the combined line shape to shift and to become asymmetric. The heading-error shift (difference between the central frequency and the maximum of the signal) is 12 Hz. Applying an rf field, the single peak of the optical-rotation signal appears at the central frequency again. Figure 4(b) shows the heading error as a function of the magnetic-field tilt angle in the direction of the probe beam for different amplitudes of the rf field. Without the rf field, the heading error goes linearly with the tilt angle at a rate of 1.1 Hz per degree. The slope of the heading-error shift tends to zero with an increase in the spin-locking rf amplitude. The heading-error compensation with tilt along both $\hat{x}$ and $\hat{y}$ is discussed in Supplemental Material [19].

In conclusion, a method for suppressing the NLZ effect and heading error for magnetic fields in the range of Earth's magnetic field using spin locking is demonstrated. An rf field along the $\hat{y}$ direction is applied which effectively suppresses NLZ-related broadening and heading error. The

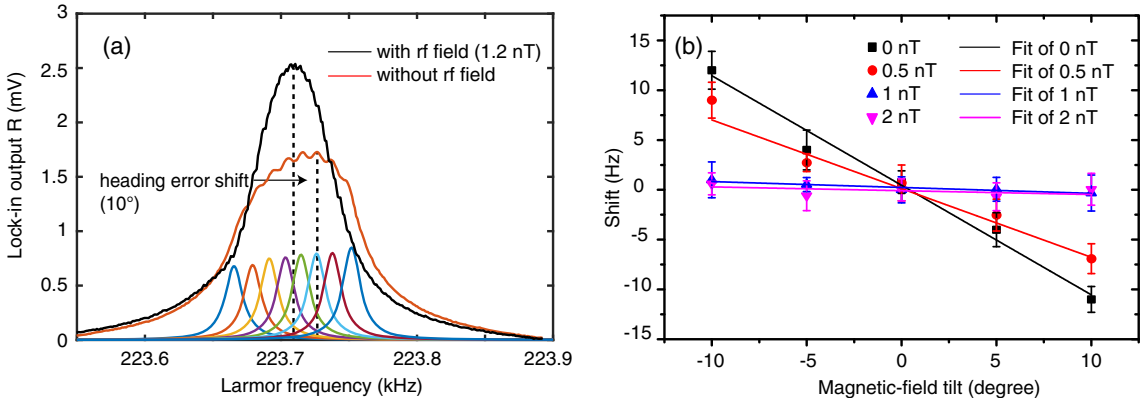

FIG. 4. (a) Optical-rotation signal amplitude for a fixed pump-modulation frequency of 223 700 Hz while scanning the magnetic field (expressed in Larmor frequency). The red curve shows the effect of a heading error for a 10° misalignment of the magnetic-field axis to the direction of the probe beam (the $\hat{x}$ axis). A tilt in the field seems to shift the center of the resonance to higher frequencies and causes a visible asymmetry in the line shape. We fit the signal with eight Lorentzian peaks. The center of the resonance is found by averaging the eight individual center frequencies. The black curve shows the magnetic resonance for the same misaligned magnetic field with an applied 1 nT spin-locking field. The resonance is symmetric with the correct central frequency. (b) Observed shift of the magnetic resonance due to a heading error as a function of the misalignment angle for different amplitudes of the spin-locking field. Without this, the heading error is about 1.1 Hz/degree, and it reduces for increasing spin-locking field amplitudes.

optimal spin-locking field corresponds to the Larmor frequency in the rotating frame comparable to the spin-revival frequency; the phase is chosen such that the corotating part of the rf magnetic field is collinear with the precessing spins. We note that the sensitivity of Earth-field magnetometers can be improved quadratically due to the increase in signal amplitude and the reduction in effective linewidth. The effect of spin-locking rf fields at frequencies different from that of the pump-modulation frequency will be assessed in future work.

The authors acknowledge support by the German Federal Ministry of Education and Research (BMBF) within the Quantumtechnologien program (FKZ 13N14439) and the DFG through the DIP program (FO 703/2-1). G. B. acknowledges support by the China Scholarship Council. W. Z. acknowledges support from National Key Research and Development Program of China under Grant No. 2016YFA0302001, the National Natural Science Foundation of China (Grants No. 11654005, No. 11234003, and No. 11129402), and the Science and Technology Commission of Shanghai Municipality (Grant No. 16DZ2260200). We thank Jason Stalnaker, Wenhao Li, Kasper Jensen, Micah Ledbetter, and Brian Patton for helpful discussions.

[1] H. Dang, A. Maloof, and M. Romalis, Appl. Phys. Lett. **97**, 151110 (2010).
[2] G. Vasilakis, J. M. Brown, T. W. Kornack, and M. V. Romalis, Phys. Rev. Lett. **103**, 261801 (2009).
[3] I. Altarev *et al.*, Phys. Rev. Lett. **103**, 081602 (2009).
[4] G. Bison, N. Castagna, A. Hofer, P. Knowles, J.-L. Schenker, M. Kasprzak, H. Saudan, and A. Weis, Appl. Phys. Lett. **95**, 173701 (2009).
[5] C. N. Johnson, P. Schwindt, and M. Weisend, Phys. Med. Biol. **58**, 6065 (2013).
[6] M. P. Ledbetter, I. M. Savukov, V. M. Acosta, D. Budker, and M. V. Romalis, Phys. Rev. A **77**, 033408 (2008).
[7] W. C. Griffith, S. Knappe, and J. Kitching, Opt. Express **18**, 27167 (2010).
[8] S. J. Smullin, I. M. Savukov, G. Vasilakis, R. K. Ghosh, and M. V. Romalis, Phys. Rev. A **80**, 033420 (2009).
[9] D. Budker and M. Romalis, Nat. Phys. **3**, 227 (2007).
[10] S. J. Seltzer, P. J. Meares, and M. V. Romalis, Phys. Rev. A **75**, 051407 (2007).
[11] V. Acosta, M. P. Ledbetter, S. M. Rochester, D. Budker, D. F. Jackson Kimball, D. C. Hovde, W. Gawlik, S. Pustelny, J. Zachorowski, and V. V. Yashchuk, Phys. Rev. A **73**, 053404 (2006).
[12] K. Jensen, V. M. Acosta, J. M. Higbie, M. P. Ledbetter, S. M. Rochester, and D. Budker, Phys. Rev. A **79**, 023406 (2009).
[13] W. Li, X. Peng, S. Li, C. Liu, H. Guo, P. Lin, and W. Zhang, in *Proceedings of the 2016 IEEE International Frequency Control Symposium (IFCS)* (IEEE, New York, 2016), pp. 1–4.
[14] E. Alexandrov, Phys. Scr. **2003**, 27 (2003).
[15] A. Ben-Kish and M. V. Romalis, Phys. Rev. Lett. **105**, 193601 (2010).
[16] A. J. Vega, J. Magn. Reson. **65**, 252 (1985).
[17] G. Breit and I. Rabi, Phys. Rev. **38**, 2082 (1931).
[18] M. Auzinsh, D. Budker, and S. Rochester, *Optically Polarized Atoms: Understanding Light-Atom Interactions* (Oxford University, New York, 2010).
[19] See Supplemental Material at http://link.aps.org/supplemental/10.1103/PhysRevLett.120.033202 for theoretical results and more details, which includes Refs. [20,21].

[20] M. Auzinsh, D. Budker, and S. Rochester, Phys. Rev. A **80**, 053406 (2009).
[21] http://rochesterscientific.com/ADM/.
[22] H. Robinson, E. S. Ensberg, and H. G. Dehmelt, Bull. Am. Phys. Soc. **3**, 9 (1958).
[23] M. Bouchiat and J. Brossel, Phys. Rev. **147**, 41 (1966).
[24] E. B. Alexandrov and V. A. Bonch-Bruevich, Opt. Eng. **31**, 711 (1992).
[25] E. B. Alexandrov, M. V. Balabas, D. Budker, D. English, D. F. Kimball, C.-H. Li, and V. V. Yashchuk, Phys. Rev. A **66**, 042903 (2002).
[26] V. V. Yashchuk, D. Budker, and J. R. Davis, Rev. Sci. Instrum. **71**, 341 (2000).
[27] D. Budker, W. Gawlik, D. Kimball, S. Rochester, V. Yashchuk, and A. Weis, Rev. Mod. Phys. **74**, 1153 (2002).